The Astrophysical Journal, 567:L000–L000, 2002 March 10

LONG-PERIOD CHROMOSPHERIC OSCILLATIONS IN NETWORK BRIGHT POINTS

R. T. James McAteer,[1] Peter T. Gallagher,[1,2] David R. Williams,[1] Mihalis Mathioudakis,[1]
Kenneth J. H. Phillips,[3] and Francis P. Keenan[1]

Received 2002 January 14; accepted 2002 February 5; published 2002 February 18

ABSTRACT

The spatial variation of chromospheric oscillations in network bright points (NBPs) is studied using high-resolution observations in Ca II K3. Light curves and hence power spectra were created by isolating distinct regions of the NBP via a simple intensity thresholding technique. Using this technique, it was possible to identify peaks in the power spectra with particular spatial positions within the NBPs. In particular, long-period waves with periods of 4–15 minutes (1–4 mHz) were found in the central portions of each NBP, indicating that these waves are certainly not acoustic but possibly due to magnetoacoustic or magnetogravity wave modes. We also show that spatially averaged or low spatial resolution power spectra can lead to an inability to detect such long-period waves.

Subject headings: Sun: chromosphere — Sun: magnetic fields — Sun: oscillations — Sun: photosphere

1. INTRODUCTION

The solar atmosphere from the photosphere to the corona has been the focus of many theoretical and observational studies. In recent years, it has become clear that the chromosphere can be divided into several distinct regions based on distinct morphological, dynamical, and physical characteristics. The internetwork, defined as regions between supergranular lanes, is now believed to be heated by upward-propagating acoustic waves, which form shocks in the increasing density gradient of the midchromosphere (Carlsson & Stein 1997; Wikstøl et al. 2000), although McIntosh et al. (2001) have suggested magneto-acoustic-gravity waves could be responsible. The solar network, defined as the boundaries of supergranular flows, contains periods longward of the acoustic cutoff and the Brunt-Väisällä cutoff (the low-frequency cutoff for gravity waves). These are not correlated with underlying fluctuations (Lites, Rutten, & Kalkofen 1993; Cauzzi, Falchi, & Falciani 2000), and their origins had been attributed to magnetic stochastic processes (Kneer & von Uexküll 1985, 1986; von Uexküll et al. 1989) or events spatially removed from the network, e.g., granular overshoot (Lites et al. 1993). In Ca II K3 (3933.7 Å), the network is only partially defined as brightenings where several supergranules meet. Due to the coincidence of these network bright points (NBPs) with high magnetic field concentrations, magnetohydrodynamic (MHD) waves (Kalkofen 1997; Hasan & Kalkofen 1999) and magnetogravity waves (Damé, Gouttebroze, & Malherbe 1984; Deubner & Fleck 1990; Kneer & von Uexküll 1993) seem to be the modes most likely present. The mechanism responsible for heating the network is still the topic of much debate, with a recent publication by Rosenthal et al. (2002) beginning to address the problem.

The existence of low-frequency oscillations in the network has been known for many years (Damé et al. 1984; Baudin, Bocchialini, & Koutchmy 1996; Rutten 1999). However, few authors have identified specific frequencies. Table 1 contains a list of the specific frequencies that have been found in the literature. Some important points concerning this table are noted here. Kalkofen (1997) points out that many of the frequencies correspond to periods that may be due to insufficiently long observing windows. Through this argument, he discounts all but the 2.7 mHz frequency in Damé et al. (1984) and that at 2.5 mHz in Lites et al. (1993). A similar argument can be used to discount the 0.6 mHz period discovered by Cauzzi et al. (2000). Furthermore, the smoothing window used by Cauzzi et al. (2000) directly affects the 1.3 mHz oscillation amplitude found by these authors. The right-hand column of Table 1 shows the frequency resolution, defined as the Nyquist frequency divided by half the number of points in the time series. With the resulting frequency resolutions, all nondiscounted frequencies can be reduced to 2.4 ± 0.3 and 3.0 ± 0.3 mHz.

The results of these studies have been based on averaging over the whole network (Damé et al. 1984), a single NBP (Lites et al. 1993; Curdt & Heinzel 1998), or the average of several NBPs (Doyle et al. 1999; Cauzzi et al. 2000). In the present Letter, we improve on these methods by using an intensity thresholding technique that allows us to identify peaks in the power spectra with particular spatial positions in each NBP. We also identify and analyze seven NBPs individually, with a higher frequency resolution and an improved filtering routine. In § 2, we briefly discuss the Ca II K3 observations used in this work, while an overview of the results is given in § 3. Sections 4 and 5 then present our discussion and conclusions.

2. OBSERVATIONS

The observations were carried out on 1998 September 22, with the Richard B. Dunn Solar Telescope (DST) at the National Solar Observatory/Sacramento Peak. The telescope was equipped with a Hallé birefringent filter and a CCD as a detector. We obtained a 150 minute sequence of $100'' \times 100''$ Ca II K3 images centered on quiet Sun (solar $X = -25''$, solar $Y = -35''$) at a 45 s cadence. The observations were taken as part of an 11 day long joint campaign with the *Transition Region and Coronal Explorer* (*TRACE*) spacecraft. The aim of the campaign was to examine the relationship between quiet Sun events in the photosphere, chromosphere, and transition region. Co-alignment of the ground-based images with the *TRACE* data led to a calculated resolution of $0\farcs33$ pixel^{-1}.

Analysis of the DST observations was carried out using standard routines within the SolarSoftWare package written in

[1] Department of Pure and Applied Physics, Queen's University Belfast, BT7 1NN Belfast, Northern Ireland, UK; j.mcateer@qub.ac.uk.
[2] Emergent Technology Services, Inc., NASA Goddard Space Flight Center, Greenbelt, MD 20771.
[3] Space Science Department, Rutherford Appleton Laboratory, Chilton, Didcot, Oxford OX11 0QX, UK.

TABLE 1
SUMMARY OF FREQUENCIES FOUND IN NETWORK REGIONS

Line	Frequencies (mHz)	Frequency Resolution (mHz)	Reference
Ca II K3	1.3, 2.0, 2.7, 3.2	0.32	1
Ca II H3[a]	0.9, 1.8, 2.5	0.27	2
Ly5, Ly9, Ly15[b]	2.2–2.4	0.24	3
N I, C II	3.0	0.27	4
Hα	0.6, 1.3, 2.2	0.34	5

[a] Velocity fluctuation.
[b] Number refers to Lyman series number.
REFERENCES.—(1) Damé et al. 1984; (2) Lites et al. 1993; (3) Curdt & Heinzel 1998; (4) Doyle et al. 1999; (5) Cauzzi et al. 2000.

IDL (Freeland & Handy 1998). The data were corrected for CCD readout bias and flat-fielded. Each image was aligned to the first image of the series by means of cross-correlation.

3. RESULTS

We have clearly identified seven NBPs throughout the entire series and have chosen subfields of $30'' \times 30''$ centered on each. Contours were drawn on each image, which confined all pixels with an intensity greater than a chosen threshold above the mean (Fig. 1*a*). This ensures that each NBP is followed correctly over time (Cauzzi et al. 2000). Here we add a further improvement to the contour method that allows us to better isolate each individual NBP. A routine was used to ensure only pixels within a closed contour around the NBP were used. This ensures that erroneous pixels—due to sudden fluctuations in the background, supergranular lane flow, or other NBPs—are ignored.

We create light curves using the following method. For a single image, *i*, a histogram of the pixel intensity is constructed, from which $I^{\rm mod}$, the most common (modal) pixel value of the image is selected to represent the background (Fig. 1*b*). A threshold pixel intensity is then chosen to contour the NBP. All pixels inside this contour are included in the NBP, and $I^{\rm ave}$ is calculated as the average pixel value of all these pixels. The contrast, C_i, of this image is then defined as

$$C_i = \frac{I_i^{\rm ave} - I_i^{\rm mod}}{I_i^{\rm ave} + I_i^{\rm mod}}. \quad (1)$$

This is repeated for every image in the sequence for a given threshold, such that the final light curve is then a series of C_i-values. This light curve construction removes any long-term trend due to sky fluctuations. The threshold value was then increased and a new light curve created. The threshold was chosen to increase from a minimum of one standard deviation (σ) above the mean, in steps of 0.05 σ. The maximum threshold chosen was that value for which the contour, in any image in the sequence, confined less than 10 pixels. This normally occurred in only one image per sequence, such that the average number of pixels in an image at maximum threshold was around 100. With this method, increasing the threshold corresponds to better isolation of the very center of the NBP (Fig. 1*a*) and provides a means of probing and comparing different parts of the NBP. Essentially, this increasing threshold creates a series of nested contours. The light curves were high-pass filtered by convolving them with a suitable Bessel function. This is the statistically preferred means of filtering any remaining very low frequencies that may dominate the power spectrum. The filter profile chosen had no effect on frequencies above 1.5 mHz and only reduces the power at 1.0 mHz to 90% of the unfiltered light curve. Frequencies lower than this may be of solar origin, but other factors such as atmospheric effects and edge effects are strong in this region, and hence these frequencies are disregarded.

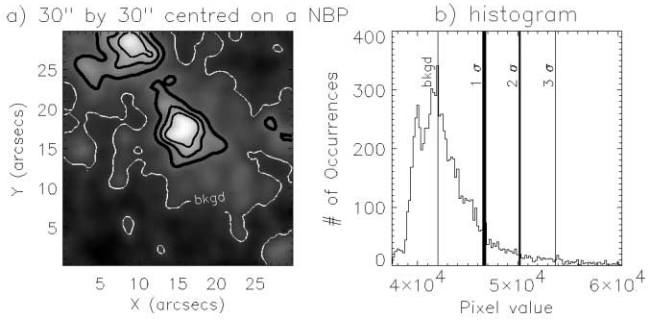

FIG. 1.—(*a*) Sample NBP. The thick lines show the contour for all pixels in the image which are 1.0 σ (*thickest line*), 2.0 σ, and 3.0 σ (*thinnest line*) above the mean. Only pixels inside the three centermost contours are included (see text). The white line contours the background level. (*b*) Corresponding histogram of the sample image. The background level is the modal value. The three vertical lines refer to the contour levels of (*a*).

Power spectra of the filtered light curves were created by using a fast Fourier transform. The Nyquist frequency of 11.1 mHz and time series of 200 data points give a frequency resolution of 0.11 mHz in the power spectrum (according to the definition in § 1), which is somewhat higher than the resolutions in Table 1.

4. DISCUSSION

In Figure 2, we show an example of how the power spectrum changes with increasing threshold. At high frequencies, the power spectra are very similar for both thresholds, while at low frequencies, they are markedly different. The power of the two largest peaks, at 3.11 and 3.33 mHz, has increased by a factor of ~2 when the higher threshold is chosen. Furthermore, a peak at 2.67 mHz has increased by a factor of ~2.5 to over 95% significance, and a peak at 2.11 mHz has increased by a factor of ~5, to well above the 99% significance level. A more

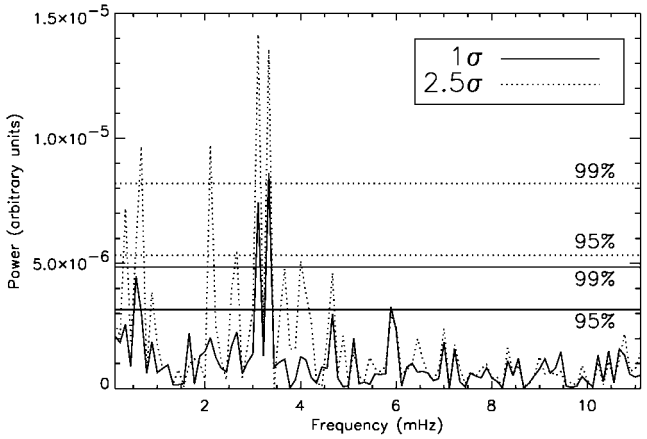

FIG. 2.—Power spectra of a single NBP at different threshold values where the solid and dotted lines refer to a threshold of 1.0 σ and 2.5 σ above the mean, respectively. The 99% and 95% significance levels are shown, corresponding to the levels at which 1% and 5% of data points, respectively, are expected to be due to random fluctuations.

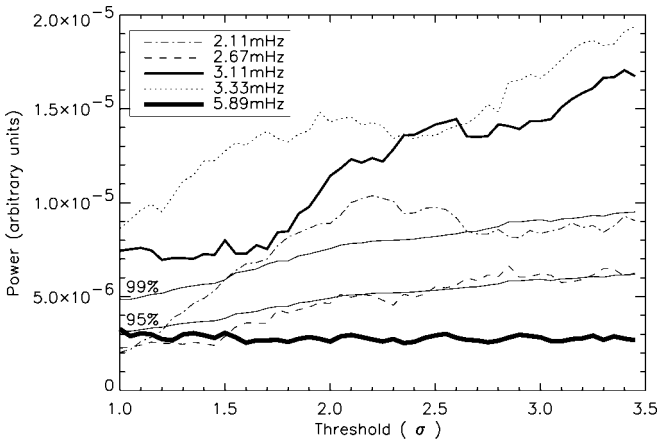

FIG. 3.—Power against threshold for the NBP of Fig. 1. The *x*-axis gives the threshold in terms of σ above the mean. The 99% and 95% levels are also shown for each threshold

detailed graph showing the development of peaks with increasing threshold is given in Figure 3. This shows quite clearly the appearance of a 2.11 mHz oscillation at ~1.5 σ, peaking in power at ~2.5 σ before leveling off around the 99% significance level. The 3.33 and 3.11 mHz frequencies more than double in power from minimum to maximum threshold. A 2.67 mHz frequency also appears, but only to the 95% significance level, while the higher value of 5.89 mHz (although staying at a similar power) becomes less statistically significant. Similar behavior is repeated in all the other NBPs but for different frequencies. The fact that no single specific frequency dominates throughout the network, combined with the lack of this behavior in internetwork regions, suggests that this is a real effect. A summary of the frequencies found in each NBP is shown in Table 2. In this table, the error is taken to be the frequency resolution (i.e., ± 0.11 mHz). There are two distinct types of behavior described in this table. Some frequencies show a steady increase in power with increased threshold and are confined to the center of the NBP. These are denoted "*s*." Other frequencies showed a steady increase up to a threshold value, after which there is a plateau in power (or slight decrease). These are denoted as "*p*." The "99" and "95" labels refer to the fact that the power of the frequency reached higher than the 99% and 95% significance levels, respectively. Frequencies at the 95% significance level which only exist for a small range of threshold values are not included, as they may be random effects, although we note the possibility of frequencies only existing in a very small part of an NBP.

In some cases, the onset of low-frequency oscillations coincides with the disappearance of higher frequencies (Fig. 3), suggesting that gravity or magnetism is the dominant restoring force in the center of NBPs, at the expense of weaker acoustic waves. Lou (1995) suggested that diverging magnetic flux tubes in the chromosphere and lower corona form a magnetic bottle that can trap magnetogravity modes. This scenario can create long-period oscillations in the range 1200–200 s (0.8–5.0 mHz) in the chromospheric network. Although all frequencies found here fall within this range, they are also consistent with MHD waves in NBPs. Kalkofen (1997) shows how fast-mode MHD waves (where magnetism is the dominant restoring force), at frequencies greater than ~1.3 mHz (less than half the acoustic cutoff frequency), can be excited by granular buffeting (Hasan & Kalkofen 1999). These propagate upward and couple with

TABLE 2

SUMMARY OF FREQUENCIES (mHz) FOUND IN THE SEVEN NBPS, THEIR SIGNIFICANCE, AND BEHAVIOR AS A FUNCTION OF THRESHOLDING INTENSITY[a]

1.11	1.56	1.89	2.22	2.78	3.11	3.33	3.78
…	…	…	99*p*	95*s*	99*s*	99*s*	…
…	95*p*	…	95*s*	99*s*	99*s*	99*s*	99*p*
95*s*	99*s*	…	…	99*s*	95*s*	99*s*	…
…	…	…	95*s*	95*s*	95*p*	…	99*p*
99*p*	…	…	99*p*	…	…	99*p*	95*p*
99*p*	…	…	95*p*	99*s*	…	99*p*	95*s*
99*p*	…	99*p*	99*s*	…	…	…	…

[a] See text for details.

weaker slow-mode MHD waves (where pressure is the dominant restoring force) at a higher frequency of ~3.4 mHz (just above the acoustic cutoff frequency), thereby transferring power to the slow-mode waves. These longitudinal slow-mode waves become shocks, thereby heating the upper chromosphere. Ulmschneider, Zähringer, & Musielak (1991) show that during coupling a fast-mode wave at frequency ν will transfer most of its energy to a slow-mode wave at frequency 2ν, although some energy will be left in waves at the original frequency ν. This agrees with Table 2, where the weaker, less common, lower frequencies may be the signature of the fast-mode waves.

It can clearly be seen from Figure 4 that particular frequencies may dominate in different areas of an NBP. At maximum threshold, the 3.33 mHz frequency dominates (point D). With smaller threshold, hence including more of the edge of the NBP, 2.89 mHz (point C), 3.89 mHz (point B), and 3.11 mHz (point A) dominate in turn. As these incremented thresholds refer to a series of nested contours, this highlights how the power spectrum is highly dependent on the chosen threshold value.

We wish to emphasize that when the entire $100'' \times 100''$ image is used to create light curves using a similar method (i.e., summing over all NBPs), it is the ~2.22 mHz (steadily increases) and ~1.00 mHz (plateaus) frequencies that dominate. This agrees with the results of Lites et al. (1993), who use only one NBP, and Cauzzi et al. (2000), who used the average of 11.

The 3.33 mHz frequency (5 minute) is well known and has

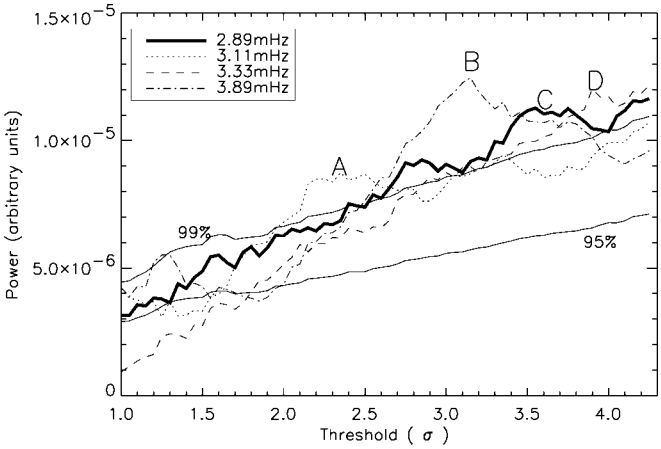

FIG. 4.—Power against threshold for the second NBP in Table 2. Labels A, B, C, and D refer to the points in the diagram where different frequencies dominate.

been previously reported in solar network regions (Kneer & von Uexküll 1993; Al, Bendlin, & Kneer 1998; Bocchialini, Vial, & Koutchmy 1994; Baudin, Bocchialini & Koutchmy 1996). However, we point out that it does not appear in all NBPs and in several cases is not the dominant frequency.

5. CONCLUSIONS

We have used high spatial and frequency resolution observations in Ca II K3 to analyze seven individual NBPs. The power detected is highly dependent on the thresholding intensity used to extract each light curve, and each NBP is slightly different. Frequencies detected confirm the ~2.2 and ~3.3 mHz values found previously. However, we have also detected new frequencies at 3.78, 3.11, 2.78, and 1.11 mHz in several NBPs, whereas 1.56 mHz occurs in only two NBPs and 1.89 mHz in only one. The lack of detection of these frequencies in previous studies may be due to our improved method of isolation of each NBP and a higher frequency resolution. The frequencies found agree with the existence of a magnetic component in the waves, either as magnetogravity waves or MHD waves.

Further study of a larger sample of NBPs over a longer timescale will be necessary to more accurately identify the dominant frequencies. Observations at different wavelengths will also be necessary to track these frequencies through the atmosphere and so provide a better idea of how they may be related to the chromospheric and coronal heating processes. The relationship of NBP behavior to the magnetic field strength of the underlying photosphere could prove particularly interesting.

The DST observations were obtained by P. T. G. as a visiting research student at the National Solar Observatory, National Optical Astronomy Observatories, operated by the Association of Universities for Research in Astronomy (AURA), Inc., under cooperative agreement with the National Science Foundation. This work was supported by the UK Particle Physics and Astronomy Research Council and the Northern Ireland Department of Education and Learning. We also thank Tom Berger and Ray Smartt for useful advice and discussion regarding data analysis and acquisition.

REFERENCES

Al, N., Bendlin, C., & Kneer, F. 1998, A&A, 336, 743
Baudin, F., Bocchialini, K., & Koutchmy, S. 1996, A&A, 314, L9
Bocchialini, K., Vial, J.-C., & Koutchmy, S. 1994, ApJ, 423, L67
Carlsson, M., & Stein, R. F. 1997, ApJ, 481, 500
Cauzzi, G., Falchi, A., & Falciani, R. 2000, A&A, 357, 1093
Curdt, W., & Heinzel, P. 1998, ApJ, 503, L95
Damé, L., Gouttebroze, P., & Malherbe, J.-M. 1984, A&A, 130, 331
Deubner, F.-L., & Fleck, B. 1990, A&A, 228, 506
Doyle, J. G., van den Oord, G. H. J., O'Shea, E., & Banerjee, D. 1999, A&A, 347, 335
Freeland, S. L., & Handy, B. N. 1998, Sol. Phys., 182, 497
Hasan, S. S., & Kalkofen, W. 1999, ApJ, 519, 899
Kalkofen, W. 1997, ApJ, 486, L145
Kneer, F., & von Uexküll, M. 1985, A&A, 144, 443
Kneer, F., & von Uexküll, M. 1986, A&A, 155, 178
———. 1993, A&A, 274, 584
Lites, B. W., Rutten, R. J., & Kalkofen, W. 1993, ApJ, 414, 345
Lou, Y. Q. 1995, MNRAS, 274, L1
McIntosh, S. W., et al. 2001, ApJ, 548, L237
Rosenthal, C. S., et al. 2002, ApJ, submitted
Rutten, R. J. 1999, in ASP Conf. Ser. 184, Third Advances in Solar Physics Euroconference: Magnetic Fields and Oscillations, ed. B. Schmieder, A. Hoffman, & J. Staude (San Francisco: ASP), 181
Ulmschneider, P., Zähringer, K., & Musielak, Z. E. 1991, A&A, 241, 625
von Uexküll, M., Kneer F., Malherbe, J. M., & Mein, P. 1989, A&A, 208, 290
Wikstøl, O., Hansteen, V. H., Carlsson, M., & Judge, P. G. 2000, ApJ, 531, 1150